Photothermal Nanoconfinement Reactor: Boosting Chemical Reactivity with Locally High Temperature in a Confined Space.

A Journal of the Gesellschaft Deutscher Chemiker

Angewandte International Edition GDCh Chemie

www.angewandte.org

Accepted Article

Title: Photothermal Nanoconfinement Reactor: Boosting Chemical Reactivity with Locally High Temperature in a Confined Space

Authors: Han-Chao Zhang, Zhan-Xiao Kang, Jiang-Jin Han, Peng Wang, Jin-Tu Fan, and Guo-Ping Sheng

To be cited as: *Angew. Chem. Int. Ed.* **2022**, e202200093

Link to VoR: https://doi.org/10.1002/anie.202200093

WILEY-VCH

10.1002/anie.202200093

WILEY-VCH

RESEARCH ARTICLE

Photothermal Nanoconfinement Reactor: Boosting Chemical Reactivity with Locally High Temperature in a Confined Space

Han-Chao Zhang[1,2,3], Zhan-Xiao Kang[2], Jiang-Jin Han[1], Peng Wang[3]*, Jin-Tu Fan[2], Guo-Ping Sheng[1]*,

*Corresponding author:
Prof. Guo-Ping Sheng
1. CAS Key Laboratory of Urban Pollutant Conversion, Department of Environmental Science and Engineering, University of Science and Technology of China, Hefei, 230026, Peoples R China
Fax: +86-551-63607453
E-mail: gpsheng@ustc.edu.cn
2. Institute of Textiles and Clothing, Hong Kong Polytechnic University, Kowloon, Hong Kong 999077, Peoples R China
Prof. Peng Wang
3. Department of Civil & Environmental Engineering, Hong Kong Polytechnic University, Kowloon, Hong Kong 999077, Peoples R China
Fax: +852 2766 6067
E-mail: peng1.wang@polyu.edu.hk

Abstract: Herein, a photothermal nanoconfinement reactor (PNCR) system is proposed and demonstrated by using hollow carbon nanospheres (HCN) to enhance the performance of chemical reaction. Under light irradiation, the local temperature of HCN inner void space was much higher than the bulk solution temperature because the confined space concentrates heat and inhibits heat loss. Using a temperature sensitive model reaction, peroxydisulfate (PDS) activation to oxidize micropollutant, it is shown that the degradation rate of sulfamethoxazole in the PNCR system was 7.1 times of those without nanoconfinement. It is further discovered that the high-quality local heat inside the nanoconfined space shifted the model reaction from an otherwise non-radical pathway to a radical-based pathway in the presence of the confinement. This work provides an interesting strategy to produce locally high temperature which has a wide range of applications to energy and environmental fields.

Introduction

Enhancing reaction rate and selectivity are two main goals for the chemical reactions.[1] Based on Arrhenius formula, reaction rate is positively related to the reaction temperature. High reaction temperature has shown to help overcome reaction activation barrier and enhance product selectivity for such catalytic reactions as ammonia synthesis[2] and selective hydrogenation.[3] Recently, light has been widely investigated as a non-contacting and convenient energy source to increase reaction temperature[4]. In particular, photothermal conversion material-assisted light-based heating is emerging as promising approach to remotely and precisely initiate and control chemical reactions and has found itself many interesting applications, including photothermal therapy, photocatalysis, micropollutant degradation, and CO_2 catalysis.[5]

In a typical material-assisted photothermal process, light is absorbed and transformed to heat on the surface of the photothermal materials (e.g., noble metals, carbon materials, semiconductor materials, organic materials),[6] and this surface heat would simultaneously diffused to the bulk solution driven by temperature gradient. It has been reported that most of the surface-generated heat is wasted in heating the bulk solution, instead of producing locally high temperature.[7] In an aqueous solution, due to the large specific heat capacity of water (4200 J/(kg K)), the bulk solution temperature rise would be limited, leading to unsatisfactory performance improvement of chemical reaction.

In the past years, various nanoconfinement reactors were developed for adsorption, catalysis, separation, energy storage and biomedicine.[8] In this work, a photothermal nanoconfinement reactor (PNCR) is rationally designed, with which this work is able to demonstrate, for the first time, the importance of locally high temperature within a limited number of nanoconfinement to greatly boost the overall chemical reaction rate of an otherwise large reaction volume. More specifically, hollow carbon nanospheres (HCN) is devised to serve as both photothermal and nanoconfinement components, and the void inside the HCN is the reaction hotspot. Meanwhile, the mesoporous shell of the HCN allows for easy and unimpeded transmission of reactant and products and also serves as shield for unwanted interfering species. Under irradiation, the carbon shell effectively absorbs and converts light to heat. The generated heat, majorly via conduction and thermal irradiation, heats up the inner void space to the same temperature as the photothermal shell, giving rise to a locally heated-up nanoconfinement reactor with significantly enhanced chemical reaction rates due to its high temperature.

The efficacy of the PNCR is demonstrated by employing peroxydisulfate (PDS) activation to oxidize micropollutant,[9] a temperature-sensitive model reaction,[10] as a proof of the concept. It is found in this work that the local heat inside PNCR is able to promote and regulate chemical reaction pathways of the model reaction. Moreover, the shell of PNCR can block interfering species (i.e., natural organic matter (NOM)) from entering the confinement reactor, leading to its largely unaffected performance. Overall, this work provides a new insight on creating and effectively utilizing light-transformed local heat and will inspire more research efforts to develop more advanced PNCR for the purpose of enhancing chemical reaction performance and beyond.

10.1002/anie.202200093

Results and Discussion

The HCN was synthesized by a hard template method, using nano-SiO_2 as template (details were provided in Supporting Information). The nano-SiO_2 was prepared by the Stöber method, followed by surface coating of polydopamine via auto-polymerization. After annealing and removing SiO_2 template by HF, the HCNs were finally synthesized by pyrolysis under different temperature.[11] The X-ray photoelectron spectroscopy (XPS) spectra of HCN shows only C, N, and O elements on the HCN surface (Figure 1a). Furthermore, no peak at 100 eV (Si) was found in the XPS spectrum, indicating the SiO_2 template was completely removed by the HF washing. Moreover, N1s spectra of HCN under different pyrolysis temperatures (Figure S1) could be deconvoluted into pyridinic N (398.2 eV), pyrrolic N (399.6 eV), graphitic N (400.9 eV), and nitric oxide (NO_x, 402.0 eV).[12] With the increasing pyrolysis temperature, the N content of HCN gradually decreased while the ratio of graphitic N increased (Figure S2). For the Raman spectra (Figure 1b), two peaks located at 1360 (D band) and 1590 cm^{-1} (G band) reflect the defective site and graphitic structure of HCN. With increasing pyrolysis temperature, the I_D/I_G of HCN was gradually increased, probably due to an increase in HCN graphitization degree.[13]

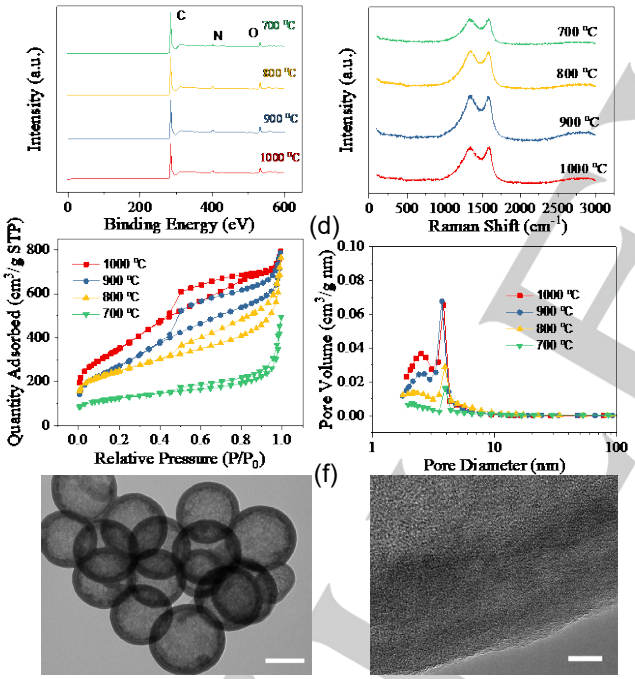

Figure 1. Characterization of HCN. The XPS survey (a); Raman spectrum (b); N_2 sorption isotherms (c); pore size distribution (d) under different pyrolysis temperatures. TEM images (e); and high-resolution TEM images (f) of HCN-1000°C, scale bars are 200 nm in (e) and 10 nm in (f).

The pore structures and specific surface areas of HCN under different pyrolysis temperatures were characterized by the N_2 sorption isotherms. As shown in Figure 1c, the N_2 sorption isotherms of HCN were classified as type IV with a H2 hysteresis loop,[14] indicating that both the microporous and mesoporous structures existed in the HCN. Importantly, plenty of mesopores located around ~2.2 nm and ~3.9 nm were observed (Figure 1d), which were conducive to the reactant and product transport in and out of PNCR during chemical reaction. Furthermore, the specific surface area of HCN was gradually increased from 432.1 to 1252.1 m^2/g with the rise of pyrolysis temperature.

The diameter of HCNs ranged from 300 to 400 nm based on the scanning electron microscope (SEM) images (Figure S3). The clear contrast between the shell and inner part of HCN under transmission electron microscopy (TEM) confirms a successful formation of the hollow structure (Figure 1e, S3). The wall thickness of HCN was approximately 30 nm based on TEM images, and the amorphous carbon structure of HCN was observed by the high-resolution TEM images (Figure 1f). Moreover, the porous structure of the wall was observed clearly in the HADDF-STEM images (Figure S3i). Furthermore, the EDX mapping (Figure S3 j, k, l, m) shows the C, N, and O elements was evenly distributed on the HCN surface.

The light absorbance results (Figure 2a) reveal dry HCN have great light absorption capability across the spectrum from 300 to 2000 nm. As a result (Figure S4), the solution temperature with HCN concentration at 10 mg/L gradually increased in response to xenon lamp irradiation (AM1.5G, 300 mW/cm^2). Furthermore, the HCN with higher pyrolysis temperature leading to the increase of the bulk solution heating rate and the final equilibrium temperature (Figure 2b) during the photothermal process, which was consistent with the light absorption by these materials (Figure 2a). During the photothermal process, the heat generated on the HCN surface gradually diffused to its inner and outer space. Only a tiny amount of water is present inside the inner confinement of HCN and needs to be heated up, in comparison to a vast volume of the bulk water outside of HCN. Therefore, the temperature in the inner space of HCN is expected to be much higher than that in the bulk solution. Regrettably, it is impossible to directly measure the accurate temperature in the inner space of each HCN due to its small size. Therefore, a numerical simulation was conducted in this work to study the temperature change and variation in the inner void, shell and outside of HCN. As shown in Figure 2c and d, the temperature of water around HCN is homogeneous and equal to the ambient temperature (25°C) initially (0 s). After 60 min of light irradiation, the temperature right on the HCN surface and its inner void space reached 69°C (Figure 2d), while the bulk solution temperature decreased sharply as the distances away from the HCN surface increases. Although this simulation did not consider the interaction among multiple particles and light scattering, it is sufficient to prove that the temperature in the inner space of HCN is much higher than the bulk solution under light irradiation. Meanwhile, the simulation results also revealed the velocity of water molecular adjacent to HCN is greatly increased due to the local temperature rise (Figure 2d), which would presumably promote local mass transfer kinetics.

Next, to demonstrate easy mass transfer of molecule with a suitable size, the uptake of fluorescein isothiocyanate (FITC) by HCN and SCN (solid carbon nanospheres, namely the same carbon spheres before removing nano-SiO_2 template) (Figure S5) was conducted and compared by the super-resolution confocal fluorescence microscope. The FITC (Mw = 389) was chosen due to its similar molecular weight and size to many micropollutants and strong fluorescent signal. As shown in Figure S5, after the experiment, the fluorescence intensity of the individual HCN

10.1002/anie.202200093

particles was much higher than that of SCN, suggesting that more FITC was contained inside HCN than SCN. Since there was no difference in the surface properties (i.e., zeta potential) between HCN and SCN (Figure S6), the higher uptake capacity of HCN was attributed to the inner void space of HCN, implying successful transfer of FITC inside the reactor from the bulk solution.

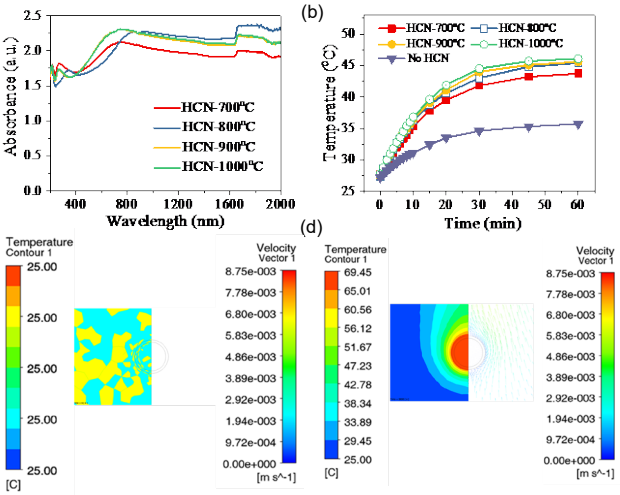

Figure 2. Light absorbance of HCN (a); the solution temperature of HCN solution (10 mg/L) under irradiation (b); numerical simulation of the temperature distribution and velocity vectors around the HCN single particle at the initial time 0 s (c) and 3600 s (d) under the irradiation.

In this work, PDS activation for micropollutants degradation, was selected to prove the effectiveness of the PNCR design. PDS is a green oxidant, which can be activated by various technologies (i.e., alkali, ultraviolet (UV), metal oxide, and carbon materials)[15] to generate reactive oxidation species (e.g., ·OH, $SO_4^{\cdot-}$, $^1O_2$). Interestingly, it has been reported that PDS can also be activated by heat to generate ·OH and $SO_4^{\cdot-}$[16], which makes PDS activation a perfect fit in PNCR. It is expected that the high-quality local heat in the inner void of PNCR system would greatly accelerate the PDS activation efficiency for the removal of micropollutants.

As shown in Figure 3a, in the dark condition, HCN alone could directly activate PDS to degrade 23.5% sulfamethoxazole(SMX), a widely detected antibiotic in the actual aquatic environment[17], during 30 min. Under the irradiation, PDS in the absence of HCN was directly activated by the UV in the simulated solar spectrum (AM1.5G) to degrade 26.4% of SMX during 30 min. Nevertheless, in the HCN photothermal activated PDS process, 95% SMX was degraded in 30 min, which was much higher than the sum of UV and HCN activation efficiency. These results indicate the SMX degradation by the PDS activation was greatly accelerated by the photothermally produced heat. Moreover, the HCN prepared at a higher synthesis pyrolysis temperature shows a better performance for the PDS activation to remove SMX both under the dark and light, probably due to the enhanced graphitization degree and photothermal property (Figure S7). The photothermal conversion of carbon material is attributed to its π-band's optical transition,[18] and the higher graphitization degree would result in more sp2 structure and more π-bands in the carbon material, which enhances its photothermal conversion performance. The UV-Vis-IR measurements confirmed that HCN produced under higher pyrolysis temperature had a better light absorption capacity (Figure 2a), which facilitates PDS activation and subsequent micropollutant degradation. Thus, the HCN-1000°C was selected as the main PNCR in the following experiments.

The solution temperature under the irradiation with UV shielded (>420 nm) showed insignificant change (Figure S8) in comparison to the one under the full spectrum (Figure 2b), while the pseudo first order reaction rate constant of SMX degradation under otherwise the same irradiation was decreased, confirming UV's contribution to the PDS activation (Figure 3b). To elaborate the effect of local heat inside PNCR on the PDS activation to degrade SMX, a water bath experiment was conducted to simulate the solution temperature change (>420 nm, Figure S8) during the photothermal process (Figure 3b). Although the SMX degradation with HCN was enhanced by heating using the water bath in the absence of light irradiation, the SMX degradation rate constant was still much lower than that under light even though they both had the same bulk solution temperatures (Figure 3b, S9). This result serves as a convincing evidence in support of that the local heat in the inner void of HCN did promote the PDS activation for the SMX degradation. Very importantly, in a sharp contrast, the SMX degradation rate under light (>420 nm) in the SCN activated PDS system shows no difference compared with that of the water bath heating (Figure 3b, S10), clearly indicating that the confined space and thus locally high temperature inside the HCN is crucial to the promotion of chemical reaction.

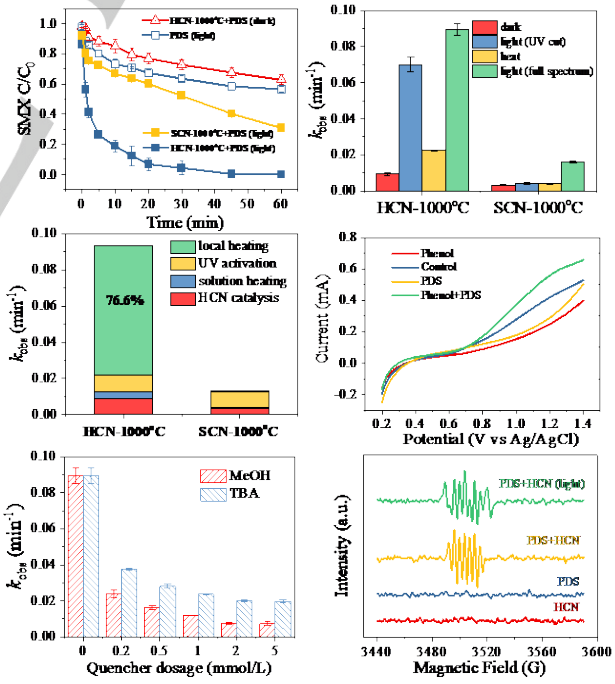

Figure 3. SMX degradation kinetics by PDS at different conditions (a); the pseudo first order reaction constant of SMX degradation in the HCN-1000°C or SCN-1000°C activated PDS under different conditions (b); The contribution of four processes on the SMX degradation in the HCN-1000°C or SCN-1000°C activated PDS system under the irradiation (c); Linear sweep voltammetry obtained by the HCN-1000°C electrode in the presence of PDS and phenol (d);The quenching effect of gradient dosage of MeOH and TBA on the SMX degradation by the PDS activated by the

HCN under irradiation (e); Electron paramagnetic resonance spectra of HCN-1000°C activated PDS under different conditions by using the DMPO as the trapping agent (f). Reaction conditions: [HCN] = 10 mg/L, [PDS] = 1 mmol/L, [SMX] = 2 mg/L, [phenol] = 10 mg/L, [DMPO] = 5.0 mmol/L, [TEMP] = 15 mmol/L, pH 7.0.

In the PNCR process, four major processes are present to activate PDS: UV activation, HCN catalytic activation (i.e., carbon material-based activation), bulk solution heating activation, and the local heat in the confined inner space of HCN for the PDS activation. The contribution of these four processes on the PDS activation was then calculated and shown in Figure 3c (details were provided in Supporting Information). As seen, the confined heat inside PNCR makes a dominant contribution of 76.6% to the SMX degradation by the PDS. It indicates the confinement space of HCN enhances the local heat utilization and provides an ideal space for the PDS activation and SMX degradation.

Moreover, the PNCR design improved the mineralization extent of SMX by 5.2 times in comparison to that under the dark (Figure S11), leading to a more complete SMX removal. Besides SMX, the PNCR system was also efficient to degrade others micropollutants, such as ampicillin (Amp), penicillin (Pen) and carbamazepine (CBZ) (Figure S12). With PNCR, the degradation rate constants of these micropollutants under irradiation were 6.48-12.76 times of those in the dark, suggesting the design of PNCR is generally applicable to various micropollutant degradation.

To confirm the reaction mechanisms behind the PNCR-assisted pollutant degradation, radicals quenching experiments by using methyl alcohol (MeOH) and tertiary butanol (TBA) were conducted to investigate the main reactive species under dark and irradiation conditions. MeOH is able to quench $SO_4^{\cdot-}$ ($k_{SO4\cdot-}$ = 1.6×10^9 M^{-1} s^{-1}) and ·OH ($k_{\cdot OH}$ = 1.9×10^9 M^{-1} s^{-1}), while TBA is only effective towards ·OH ($k_{\cdot OH}$ = 6×10^8 M^{-1} s^{-1})[19]. Under dark condition, the SMX degradation was not at all inhibited by MeOH or TBA (Figure S12), indicating the radicals were not the main reactive oxidation species in HCN activated PDS process. Furthermore, dosing D_2O to extend the lifetime of $^1O_2$[20] also shows little influence on the SMX degradation (Figure S13), indicating a minor role of $^1O_2$ in the HCN activated PDS process for the SMX degradation. Besides radicals and $^1O_2$, the mediated electron transfer is a possible oxidation mechanism. To explore this possibility, a layer of HCN was coated onto a fluorine doped tin oxide (FTO) glass, which was then used as a work electrode to evaluate electron transfer between HCN with the PDS/micropollutant (i.e., phenol) by linear sweep voltammetry (LSV) test. It is noteworthy that the phenol was selected as the model pollutant in the LSV measurement due to its reversible reduction capacity and unique oxidation peak location. As shown in Figure 3d, the current of phenol oxidation peak was greatly increased upon PDS addition, suggesting that PDS promoted electron transfer from phenol to HCN, and the mediated electron transfer was the main oxidation mechanism for HCN activated PDS process under dark.

However, in the photothermal HCN activated PDS system (Figure 3e), the SMX degradation was gradually inhibited after adding MeOH and TBA, and the quenching effect of MeOH at each dosage (0.2-5.0 mol/L) was higher than that of TBA, indicating that the $SO_4^{\cdot-}$ is the main radicals in the photothermal HCN activated PDS process. Electron paramagnetic resonance (EPR) experiment was subsequently conducted to identify the reactive oxidation species. Using 5,5-dimethyl-1-pyrroline-N-oxide (DMPO) as trap agent, a series of peaks attributed to the DMPOX were observed in the HCN activated PDS system under the dark (Figure 3f), implying that the non-radical pathway was the main mechanism in this system. Under irradiation, several peaks attributed to $DMPO_{\cdot OH}$ (hyperfine splitting constants of α_N = $\alpha_{\beta\text{-}H}$ = 14.9 G) and $DMPO_{SO4\cdot-}$ (hyperfine splitting constants of α_N = 13.2 G, $\alpha_{\beta\text{-}H}$ = 9.6 G, $\alpha_{\gamma\text{-}H1}$ = 1.48 G and $\alpha_{\gamma\text{-}H2}$ = 0.78 G)[21] were observed (Figure 3f), indicating $SO_4^{\cdot-}$ was the main oxidation species in the photothermal HCN activated PDS system. Moreover, the EPR experiment by using the 2,2,6,6-tetramethyl-4-piperidinol (TMP) as trapping agent revealed that no $^1O_2$ was generated in the HCN activated PDS system under the dark and irradiation (Figure S14). These results confirm that HCN directly activates PDS through the electron transfer mechanism in the dark, while under irradiation the main oxidation species is shifted to a radical-based process. Based on the above results, the high-quality local heat in the confinement space of HCN facilitates these reactions in need of high temperature and can regulate the pathway of chemical reactions.

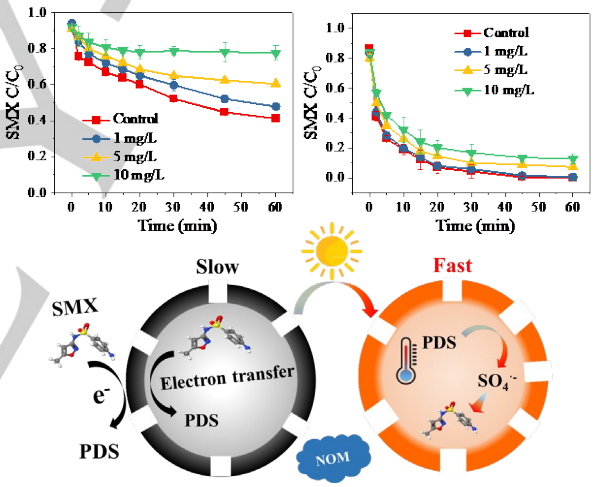

Figure 4. Effect of SRNOM on the SMX degradation by the HCN-1000°C (a) and SCN-1000°C (b) activated PDS under irradiation; Schematic diagram of this PNCR system (c). Reaction conditions: [HCN] = 10 mg/L, [PDS] = 1 mmol/L, [SMX] = 2 mg/L, pH 7.0.

Besides promoting temperature-sensitive reaction, the pores of HCN shell can be species-selective via size exclusion. For many environmental catalytic reaction, NOM ubiquitous in natural aquatic environment can quench many reactive oxidation species like ·OH (1.6-3.3 × 10^8 mol-C^{-1} s^{-1}) and $SO_4^{\cdot-}$ (2.5-8.1 × 10^7 mol-C^{-1} s^{-1})[22]. This is one of the main reasons behind significantly reduced performance of many environmental catalysis reactions when working with natural water matrix. However, in this work, it was found that the SRNOM (Suwannee River Natural Organic Matter) had insignificant influence on PNCR activated PDS to degrade SMX. As shown in Figure 4, 1 mg/L of SRNOM showed no influence on the SMX degradation (Figure 4a), and only 28.9% of SMX degradation was inhibited at 10 mg/L of SRNOM in the PNCR activated PDS system. In a sharp contrast, there was 87.5% of SMX degradation reduction in the presence of 10 mg/L of SRNOM for the SCN photothermal activated PDS process

(Figure 4b). The results convincingly show PNCR system could shield the quenching effect of NOM on the SMX degradation presumably through its mesoporous shell structure to deny the entry of the macromolecules via size exclusion. Furthermore, the local high temperature of HCN surface would facilitate the desorption of physically adsorbed NOM, thereby reducing its influence on the micropollutant degradation. Therefore, the PNCR reported in this work has a potential to reduce the negative effect of matrix in the actual water. The species-selectivity of PCNR can be further improved by precisely devising and modulating the shell pore size via template method. However, the mesopores of HCN in the current work has not selectivity and shielding effect towards HCO_3^- , which showed adverse effect on SMX degradation by the PDS activated by HCN under irradiation (Figure S15a), probably due to that the $SO_4^{\cdot-}$ could be quenched by HCO_3^- to generate the less powerful oxidant: $HCO_3^{\cdot}$. Meanwhile, the effect of Cl^- on the SMX degradation under irradiation was much low (Figure S15b). Moreover, the SMX degradation efficiency in this PNCR system was gradually decreased with the number of cycles (Figure S16) increased. Nevertheless, the performance could be largely regenerated by an annealing process. The morphology of HCN as characterized by TEM shows no significant change after the reactions (Figure S17). However, the I_D/I_G in the Raman spectra and the oxygen content of HCN were increased after the reactions (Figure S18), indicating HCN surface was oxidized by the radicals during the SMX degradation process.[23] Overall, compared to the similar materials/reactions in the literatures (Table S1), the PNCR system reported in this work significantly enhances micropollutants degradation efficiency at a low catalyst dosage condition, which can be translated to reduced operational cost in practical application.

Conclusion

A PNCR comprising HCN and activated PDS was utilized to degrade micropollutants. The PNCR enables a small volume of the void inner space of HCN to be selectively and efficiently heated up. The locally high temperature inside the HCN greatly enhanced micropollutant degradation and modulated degradation pathways, leading to a deeper degradation of the micropollutants. The shell of HCN was able to shield macromolecular species from adversely affecting the reaction within the confined reaction space, leading to a stable reaction performance. Thus, it is reasonable to believe that the confined space of HCN would provide an ideal space for various chemical reactions. The local temperature in the confined space greatly enhances the reaction rate and is more selective to the chemical reactions for which a high temperature is preferred. These results will inspire further research in the precise utilization of light energy to mediate chemical reactions in confined spaces.

Acknowledgements

The authors wish to thank the National Natural Science Foundation of China (51825804, 51821006), the Fundamental Research Funds for the Central Universities (WK2400000001) for the partial support of this study, and the startup fund at The Hong Kong Polytechnic University.

Conflict of interest

The authors declare no conflict of interest.

Keywords: confinement, photothermal, chemical reaction, persulfate activation, micropollutant, local temperature

Reference

[1] a) E. M. Simmons, J. F. Hartwig, *Nature* **2012**, *483*, 70-73; b) J. Wei, S. N. Qin, J. Yang, H. L. Ya, W. H. Huang, H. Zhang, B. J. Hwang, Z. Q. Tian, J. F. Li, *Angewandte Chemie-International Edition* **2021**, *60*, 9306-9310; c) V. K. Sharma, L. Chen, R. Zboril, *Acs Sustainable Chemistry & Engineering* **2016**, *4*, 18-34.

[2] L. Hollevoet, F. Jardali, Y. Gorbanev, J. Creel, A. Bogaerts, J. A. Martens, *Angewandte Chemie-International Edition* **2020**, *59*, 23825-23829.

[3] a) C. Q. Song, X. Liu, M. Xu, D. Masi, Y. G. Wang, Y. C. Deng, M. T. Zhang, X. T. Qin, K. Feng, J. Yan, J. Leng, Z. H. Wang, Y. Xu, B. H. Yan, S. Y. Jin, D. S. Xu, Z. Yin, D. Q. Xiao, D. Ma, *Acs Catalysis* **2020**, *10*, 10364-10374; b) Y. F. Xu, P. N. Duchesne, L. Wang, A. Tavasoli, A. A. Jelle, M. K. Xia, J. F. Liao, D. B. Kuang, G. A. Ozin, *Nature Communications* **2020**, *11,* 5149; c) H. C. Ma, C. C. Zhao, G. J. Chen, Y. B. Dong, *Nature Communications* **2019**, *10,* 3368.

[4] H. N. Huang, R. Shi, X. R. Zhang, J. Q. Zhao, C. L. Su, T. R. Zhang, *Angewandte Chemie-International Edition* **2021**, *60,* 22963-22969.

[5] a) Q. H. Yang, Q. Xu, S. H. Yu, H. L. Jiang, *Angewandte Chemie-International Edition* **2016**, *55*, 3685-3689; b) R. Y. Li, Y. S. Shi, M. C. Wu, S. Y. Hong, P. Wang, *Nature Sustainability* **2020**, *3*, 636-643; c) R. Y. Li, Y. Shi, M. C. Wu, S. Y. Hong, P. Wang, *Nano Energy* **2020**, *67,* 104255.

[6] Y. Shi, R. Li, L. Shi, E. Ahmed, Y. Jin, P. Wang, *Advanced Sustainable Systems* **2018**, *2*, 1700145.

[7] P. Tao, G. Ni, C. Y. Song, W. Shang, J. B. Wu, J. Zhu, G. Chen, T. Deng, *Nature Energy* **2018**, *3*, 1031-1041.

[8] a) M. J. Cai, Z. Y. Wu, Z. Li, L. Wang, W. Sun, A. A. Tountas, C. R. Li, S. H. Wang, K. Feng, A. B. Xu, S. L. Tang, A. Tavasoli, M. W. Peng, W. X. Liu, A. S. Helmy, L. He, G. A. Ozin, X. H. Zhang, *Nature Energy* **2021**, *6*, 807-814; b) J. Liu, N. P. Wickramaratne, S. Z. Qiao, M. Jaroniec, *Nature Materials* **2015**, *14*, 763-774; c) C. Dong, Q. Yu, R. P. Ye, P. P. Su, J. Liu, G. H. Wang, *Angewandte Chemie-International Edition* **2020**, *59*, 18374-18379; d) H. Tian, J. Liang, J. Liu, *Advanced Materials* **2019**, *31,* 1903886.

[9] a) H. C. Zhang, P. C. Guo, X. Zhang, G. P. Sheng, *Chemical Engineering Journal* **2021**, *403,* 126324; b) H. R. Wei, S. K. Loeb, N. J. Halas, J. H. Kim, *Proceedings of the National Academy of Sciences of the United States of America* **2020**, *117*, 15473-15481; c) R. L. Yin, B. H. Jing, S. X. He, J. Y. Hu, G. Lu, Z. M. Ao, C. Y. Wang, M. S. Zhu, *Water Research* **2021**, *190,* 116720.

[10] Y. F. Ji, Y. Fan, K. Liu, D. Y. Kong, J. H. Lu, *Water Research* **2015**, *87*, 1-9.

[11] C. Liu, J. Wang, J. S. Li, R. Luo, J. Y. Shen, X. Y. Sun, W. Q. Han, L. J. Wang, *Acs Applied Materials & Interfaces* **2015**, *7*, 18609-18617.

[12] Z. Q. Sun, L. Zhao, C. H. Liu, Y. F. Zhen, J. Ma, *Environmental Science & Technology* **2019**, *53*, 10342-10351.

[13] A. Jorio, R. Saito, *Journal of Applied Physics* **2021**, *129*, 021102.

[14] J. S. Im, S. J. Park, Y. S. Lee, *Journal of Colloid and Interface Science* **2007**, *314*, 32-37.

[15] J. L. Wang, S. Z. Wang, *Chemical Engineering Journal* **2018**, *334*, 1502-1517.

[16] R. H. Waldemer, P. G. Tratnyek, R. L. Johnson, J. T. Nurmi, *Environmental Science & Technology* **2007**, *41*, 1010-1015.

[17] J. F. Yan, J. L. Peng, L. D. Lai, F. Z. Ji, Y. H. Zhang, B. Lai, Q. X. Chen, G. Yao, X. Chen, L. P. Song, *Environmental Science & Technology* **2018**, *52*, 14302-14310.

[18] J. U. Kim, S. Lee, S. J. Kang, T. I. Kim, *Nanoscale* **2018**, *10*, 21555-21574.

[19] P. Neta, R. E. Huie, A. B. Ross, *Journal of Physical and Chemical Reference Data* **1988**, *17*, 1027-1284.

[20] C. M. Sharpless, *Environmental Science & Technology* **2012**, *46*, 4466-4473.

[21] P. L. Zamora, F. A. Villamena, *Journal of Physical Chemistry A* **2012**, *116*, 7210-7218.

[22] J. Lee, U. von Gunten, J. H. Kim, *Environmental Science & Technology* **2020**, *54*, 3064-3081.

[23] a) S. Ye, W. W. Shi, Y. Liu, D. F. Li, H. Yin, H. B. Chi, Y. L. Luo, N. Ta, F. T. Fan, X. L. Wang, C. Li, *Journal of the American Chemical Society* **2021**, *143*, 12499-12508; b) A. H. Lu, T. Sun, W. C. Li, Q. Sun, F. Han, D. H. Liu, Y. Guo, *Angewandte Chemie-International Edition* **2011**, *50*, 11765-11768.

10.1002/anie.202200093

Entry for the Table of Contents

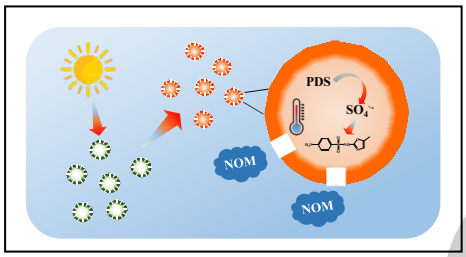

The photothermal nanoconfinement reactor (PNCR) is able to boost the overall chemical reaction rate of an otherwise large reaction volume.